Letter

Robust incoherent perfect absorption

H. S. Xu and L. Jin*
School of Physics, Nankai University, Tianjin 300071, China

(Received 8 February 2024; accepted 13 March 2024; published 5 April 2024)

A coherent perfect absorber is capable of completely absorbing input waves. However, the coherent perfect absorption severely depends on the superposition of the input waves, and the perfect absorption is sensitive to the disorder of the absorber. Thus, a robust incoherent perfect absorption, being insensitive to the superposition of input waves and the system disorder, is desirable for practical applications. Here, we demonstrate that the linearly independent destructive interference at the port connections removes the constraint on the coherent input. We propose an approach using the interplay between the loss and localization to form the incoherent perfect absorption. The resonant incidence from either port is completely absorbed. Furthermore, we utilize the lattice configuration supporting the flat band to demonstrate the disorder-immune incoherent perfect absorption. Our findings provide insight into the fundamentals and applications for the perfect absorption of light, microwaves, sound, mechanical waves, and beyond.

DOI: 10.1103/PhysRevResearch.6.L022006

Introduction. Dissipation ubiquitously exists in physical systems. Unlike the conventional wisdom to suppress dissipation, non-Hermitian optics actively engineers the dissipation and has stimulated many intriguing phenomena that have never been found in Hermitian systems. Especially, the interplay of interference and dissipation enables the complete absorption of light with the proper coherent inputs [1–15] . This phenomenon, known as coherent perfect absorption, serves as the time-reversed counterpart of lasing [16–26]. The coherent perfect absorption has immediate applications in optical switches, modulators, and imaging for the coherent control of waves [27–30]. However, the proper superposition of input waves is a prerequisite to achieve the complete absorption. This rigorous constraint on the coherent input limits the absorption efficiency and hinders the practical application of perfect absorbers [31,32]. To overcome the restriction, a unidirectional perfect absorber is designed and the input from one side is completely absorbed [33–38]. Furthermore, a bidirectional perfect absorber is capable of completely absorbing resonant input from either side [39–42]. The perfect absorption of incoherent input regardless of the superposition of incident waves is desirable. However, its design is a tough task. In addition, the perfect absorption is also sensitive to the disorder in the scattering center; any fabrication imperfection may cause the deviation from the perfect absorption.

In this Letter, we find that the linearly independent destructive interference of the degenerate eigenstates of the effective scattering center at the port connections plays an important role to overcome the constraint of perfect absorption on the coherent input, and we propose an approach to realize incoherent perfect absorption. In addition, we demonstrate the disorder-immune incoherent perfect absorption created from the compact localization of the flat band in a stub ribbon of coupled resonators. The incident waves from both ports at any superposition are completely absorbed in the presence of random coupling disorder. The proposed models can also be implemented in many experimental platforms. The formalism is applicable for many other flat-band lattices. Our findings open up an avenue in the design of highly efficient absorbers for practical applications.

Perfect absorption. In a two-port scattering system, each incident wave is split into a reflected wave and a transmitted wave after interference in the scattering center. Interestingly, the losses embedded in a non-Hermitian scattering center may completely absorb the input waves. In Fig. 1, we illustrate three types of perfect absorptions. The coherent perfect absorber realizes complete absorption of resonant input waves from both ports at a proper superposition of the wave amplitudes and phases [Fig. 1(a)]. The coherent perfect absorber is highly sensitive to the variation of input waves. The unidirectional perfect absorber realizes complete absorption of input waves from one port [Fig. 1(b)]. The unidirectional perfect absorber does not require the proper superposition of input waves, but the transmission and/or reflection for the wave injected from another port is nonzero [34–37]. Interestingly, the incoherent perfect absorber realizes complete absorption of input waves from either port [Fig. 1(c)]. The proper match of input wave amplitudes and phases is unnecessary, and any superposition of the resonant inputs from both ports can be completely absorbed. The degenerate resonances enable incoherent perfect absorbers [39].

The complete absorption of input indicates that the steady-state solution of the perfect absorber possesses the purely incoming waves at the real frequency. Notably, both the coherent perfect absorber, which requires a coherent input, and the unidirectional perfect absorber, which requires a

*jinliang@nankai.edu.cn

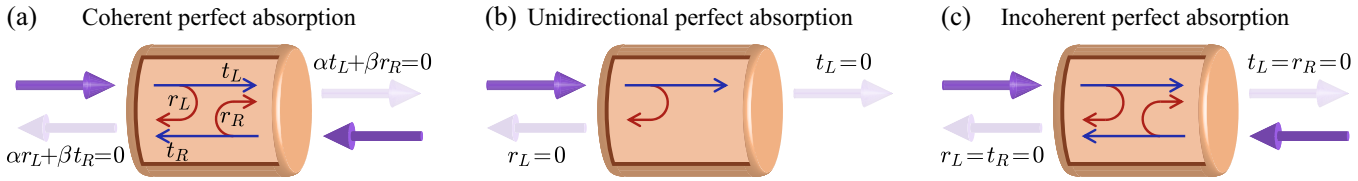

FIG. 1. Schematic of three types of perfect absorptions. (a) Coherent perfect absorption: The reflection and transmission vanish for coherent input waves from the opposite directions. The perfect absorption highly depends on the relative amplitudes and phases of input waves. (b) Unidirectional perfect absorption: The reflection and transmission vanish for input wave from one direction. (c) Incoherent perfect absorption: The output vanishes for any superposition of input waves from the opposite directions. r_L, t_L (r_R, t_R) are the reflection and transmission for the left (right) input.

specific input direction, have the nondegenerate purely incoming wave solution. By contrast, as a result of the complete absorption of incoming waves from both the left and right ports, the incoherent perfect absorber has two degenerate purely incoming wave solutions at a real frequency. This differs from the two purely incoming wave solutions coalesced to a single state [43–50], where the absorption exhibits quartic line shape. The former one is at the diabolic point of the non-Hermitian system and the latter one is at the exceptional point of the non-Hermitian system. For the incoherent perfect absorption, the incoming wave solutions from each port are linearly independent. This overcomes the constraint on the relative amplitude and phase of the input waves at the corresponding frequency.

The physical isolation between the two ports to overcome the constraint on the coherent input is not under our consideration; i.e., two decoupled single-port perfect absorbers formally combined as a two-port system apparently realize an incoherent perfect absorption. Here we highlight the interference effect in the scattering center rather than the physical isolation. Two necessary conditions are required to form incoherent perfect absorption. (i) The input frequency is the degenerate energy level of the effective scattering center, which is the scattering center with additional on-site terms reduced from the ports at the incoming wave solution. (ii) The degenerate eigenstates are able to form destructive interference at the connections, where the scattering center is connected with the ports. Then, the incoming wave is confined within each port and its extension feature is destroyed.

In our formalism, the linearly independent destructive interference at the port connections is important for the incoherent perfect absorption; i.e., two on-resonance degenerate eigenstates of the effective scattering center respectively have vanishing amplitudes at the two port connections. The microscopic origin of the degenerate resonant states differs in distinct physical systems [39]. Notably, the flat band is fully constituted by degenerate states. The flat-band eigenstates are compact localized within one or several unit cells of the lattice. The wave input on-resonance with the flat-band energy cannot propagate through the lattice. Thus, the unit cells of the flat-band lattice as the scattering center are excellent candidates to generate incoherent perfect absorption if the reflection can be perfectly absorbed via engineering the losses.

Non-Hermitian square plaquette. We consider a uniform chain of evanescently coupled resonators [Fig. 2(a)] to demonstrate the formation of incoherent perfect absorption. A non-Hermitian square plaquette is embedded in the middle of the resonator chain at two neighbor dissipative resonators; the resonators have the loss $-i\gamma$. The couplings are $-J$. The resonators have the resonant frequency ω_c and support the counterclockwise and clockwise modes, which are the time-reversal counterparts [51]. The scattering properties for the counterclockwise and clockwise mode are the same. In the coupled mode theory [35,52,53], the equation of motion for the resonator mode of the ports is

$$i\frac{df_j}{dt} = -Jf_{j-1} - Jf_{j+1}, \ (|j| > 1), \tag{1}$$

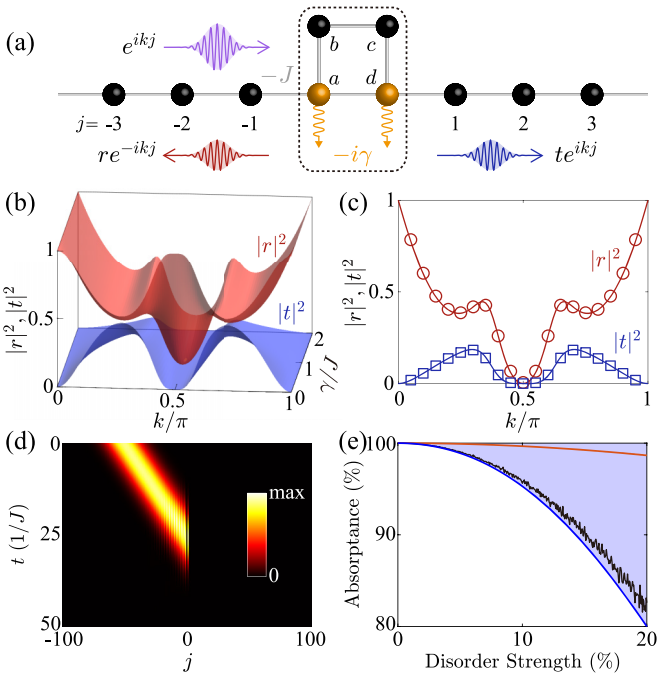

FIG. 2. (a) Schematic of a non-Hermitian square plaquette (dashed black box) embedded in the resonator array. (b) The reflection (in red) and transmission (in blue) as a function of the input wave vector and loss. (c) The reflection and transmission at $\gamma = J$. (d) The simulations of perfect absorption for the initial Gaussian wave packet centered at $N_c = -50$ with $\sigma = 10$ and $k_c = \pi/2$. (e) The absorptance as a function of disorder strength. The blue curve is the analytic result of the minimum absorptance, and the black (red) curve is the numerical result of the minimum (average) absorptance of 10^5 samples. The disorder is randomly chosen with a uniform distribution in the interval $(-1, 1)$ of disorder strength. The shaded area is the disordered absorptance range.

and

$$i\frac{df_{\mp1}}{dt} = -Jf_{\mp2} - Jf_{a(d)}, \tag{2}$$

where f_j ($|j| \geqslant 1$) is the mode amplitude for the port resonator j and f_s ($s = a, b, c, d$) is the mode amplitude for the scattering center resonator s. The resonant frequency term ω_c is removed from the equations of motion for simplicity. The system is equivalently transformed into a rotating frame with the frequency ω_c. The equations of motion for the resonator modes of the scattering center are

$$i\frac{df_a}{dt} = -Jf_d - Jf_b - Jf_{-1} - i\gamma f_a, \tag{3}$$

$$i\frac{df_b}{dt} = -Jf_a - Jf_c, \tag{4}$$

$$i\frac{df_c}{dt} = -Jf_b - Jf_d, \tag{5}$$

$$i\frac{df_d}{dt} = -Jf_c - Jf_a - Jf_1 - i\gamma f_d. \tag{6}$$

In the elastic scattering process, we have $f_{j(s)} = \psi_{j(s)}e^{-i\omega(k)t}$, where $\psi_{j(s)}$ is the steady-state wave function of the resonator. The incoming wave is reflected and transmitted by the scattering center. The steady-state solution is a superposition of two counterpropagating plane waves $e^{\pm ikj}$, where the wave momentum k is a real number. For the wave injected from the left side of the resonator array, we denote the steady-state wave function in the left port as $\psi_j = e^{ikj} + re^{-ikj}$ ($j < 0$) and the steady-state wave function in the right port as $\psi_j = te^{ikj}$ ($j > 0$), where r and t are the reflection and transmission coefficients, respectively. The scattering center has the inversion symmetry. Thus, the reflection and transmission are symmetric [54,55], being independent of the direction of the input wave.

Substituting the wave functions into Eqs. (1) and (2), we obtain the dispersion $\omega(k) = -2J\cos k$ of the ports. Substituting the wave functions into Eqs. (3)–(6), we obtain the scattering coefficients (see Supplemental Material, Sec. A [56]). The reflection and transmission as the functions of the input wave momentum k are depicted in Figs. 2(b) and 2(c). The total intensity of the scattered light is less than unity as a consequence of the losses [57]. At the resonant input $k = \pi/2$ for $\gamma = J$, the perfect absorption occurs with vanishing reflection and transmission $r = t = 0$. In this case, the scattering matrix is a 2×2 null matrix. Thus, any superposition of resonant input wave is perfectly absorbed at the non-Hermitian square plaquette, forming an incoherent perfect absorption. In Fig. 2(d), we perform the dynamics of the incoherent perfect absorption for the resonant wave injected in the left port [58]. The numerical simulations agree well with the predictions.

Incoherent perfect absorption is independent of the relative phases and amplitudes of the incoming waves from both ports and overcomes the limitation of perfect absorption being confined to coherent or unidirectional input. Nevertheless, we emphasize that the incoherent perfect absorption is still sensitive to the system parameters and the disorder in the scattering center affects the absorption efficiency. Then, the incident waves cannot be completely absorbed. Figure 2(e) shows the decreased absorptance as a function of disorder strength in the couplings of non-Hermitian square plaquettes. The minimum absorptance is 80% at a coupling disorder strength of 20% (see Supplemental Material, Sec. B [56]). The random disorder causes fluctuation in the observed minimum absorptance, which reduces as the number of samples increases.

Effective scattering center. We consider the purely incoming wave solution of the two-port non-Hermitian scattering system shown in Fig. 2(a),

$$\Psi_j = \begin{cases} \alpha e^{ikj}, & (j < 0), \\ \beta e^{-ikj}, & (j > 0), \end{cases} \tag{7}$$

where $\alpha : \beta$ indicates the relative amplitude and phase of the input waves in the left and right ports. It is important to note that any superposition of input waves from the left and right ports can be completely absorbed, making any form of $\alpha : \beta$ a perfect absorption solution for the incoherent perfect absorber. In the following analysis, the momentum k does not necessarily have to be a real number in Ψ_j.

The projection theory provides an effective Hamiltonian that equivalently describes the original system in a reduced dimension [59,60], which is the effective scattering center. From Eq. (7), the wave function continuity yielding the wave functions of the connection resonator a and d are $\Psi_a = \alpha e^{ik\cdot 0}$ and $\Psi_d = \beta e^{-ik\cdot 0}$. From Eqs. (3) and (6), the contribution of the wave function at the port to the scattering center is $-J\alpha e^{ik\cdot(-1)}$ and $-J\beta e^{-ik\cdot 1}$. From the equivalence $-J\alpha e^{ik\cdot(-1)} \equiv -Je^{-ik}\alpha e^{ik\cdot 0} = -Je^{-ik}\Psi_a$ and $-J\beta e^{-ik\cdot 1} \equiv -Je^{-ik}\beta e^{-ik\cdot 0} = -Je^{-ik}\Psi_d$, the coupling to the ports effectively reduces into the on-site term $-Je^{-ik}$ at the resonators a and d. In this scenario, the effective scattering center takes the form of

$$H_c^{\text{eff}}(k) = -\begin{pmatrix} i\gamma + Je^{-ik} & J & 0 & J \\ J & 0 & J & 0 \\ 0 & J & 0 & J \\ J & 0 & J & i\gamma + Je^{-ik} \end{pmatrix}. \tag{8}$$

The purely incoming wave solution usually corresponds to a complex frequency, which is not a steady-state solution as this leads to the input waves growing or decaying exponentially with time. However, the purely incoming wave solution can be turned to a real frequency by the loss, forming the steady-state of perfect absorption.

The effective scattering center includes the energy of the input wave, i.e.,

$$\det|H_c^{\text{eff}}(k) - \omega(k)| = 0, \tag{9}$$

where we obtain the momentum k that satisfies the purely incoming solution. We plot the solution for different loss rates γ in Fig. 3(a). When $\gamma < J$ ($\gamma > J$), there are two complex k located in the upper (lower) half plane, i.e., $\text{Im}(k) > 0$ [$\text{Im}(k) < 0$]. For $\gamma = J$, the two complex k meet on the real axis at $k = \pi/2$. The two perfect absorption solutions are degenerate and linearly independent as verified from the effective scattering center $H_c^{\text{eff}}(\pi/2)$, which has two degenerate energy levels at $\omega(\pi/2) = 0$. The corresponding degenerate eigenstates are $(1, 0, -1, 0)^T$ and $(0, -1, 0, 1)^T$, as illustrated in Fig. 3(b). Two degenerate eigenstates constitute a pair of inversion-symmetric counterparts as a consequence that the scattering center is inversion symmetric. In this case, the inversion symmetry plays an important role in the formation

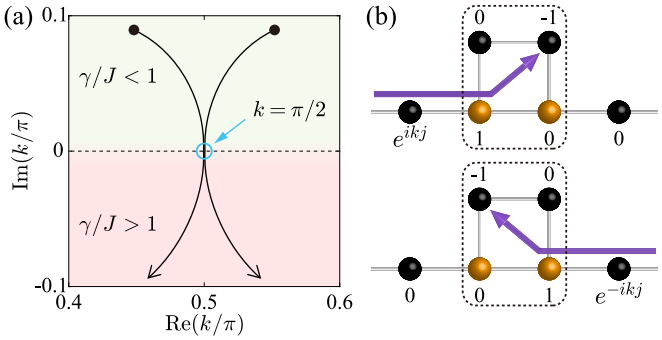

FIG. 3. The purely incoming solution of the non-Hermitian square plaquette of Fig. 2(a). (a) Trajectories of two k for the purely incoming solution as γ varies from $\gamma/J = 0$ (black solid circles) to $\gamma/J = 2$ (black arrows), and they meet at $\gamma/J = 1$ (cyan hollow circle). (b) Two degenerate eigenstates of the non-Hermitian square plaquette at $\gamma/J = 1$.

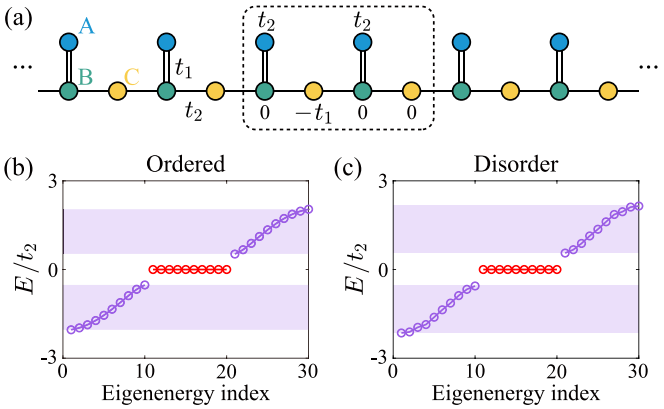

FIG. 4. (a) Schematic of the stub ribbon. The sublattices A, B, C are denoted by the blue, green, and yellow solid circles, respectively. The dashed box depicts one of the compact localized states associated with the zero-energy flat band. (b) and (c) are the eigenenergies of a 30-site stub ribbon without disorder and with disorder, respectively. The parameter is chosen $t_1 = t_2/2$. In (c), all the couplings deviate from the set parameters within the range of $[-20\%, 20\%]$.

of incoherent perfect absorption [39], which is not necessary in a more general framework. This point is demonstrated as follows.

The destructive interference of on-resonance degenerate eigenstates from the effective scattering center at a single connection resonator provides a strategy to destroy the extension feature of the perfectly absorbing state and create the incoherent perfect absorption. The localization on different ports caused by the destructive interference ensures that the incoming waves from each port are completely absorbed (see Supplemental Material, Sec. C [56]). Specifically, the nonzero wave function in the resonator a (d) represents the incoming wave from the left (right) port, while the zero wave function in the resonator d (a) causes the vanishing of the incoming wave from the right (left) port. Therefore, the scattering center independently absorbs the incoming waves from the left and right ports.

Stub ribbon. The incoherent perfect absorber is not unique. The identification of the effective scattering center holding degenerate eigenstates becomes a critical point to obtain an incoherent perfect absorber. The flat-band lattice meets the prerequisite for the incoherent perfect absorption. Notably, the dispersionless flat band holds a huge number of degenerate energy levels [61–66]. These eigenstates compactly localize within several neighbor unit cells across the lattice [67–70]. These compact localized states are linear independent. Thus, the flat-band lattice is a promising candidate for an effective scattering center. The incoherent perfect absorption is possible through engineering the losses.

We consider a stub ribbon in Fig. 4(a) [71]. The stub ribbon is a prototypical quasi-one-dimensional flat-band lattice composed of three sublattices (A, B, C) [72–75]. The sublattices have the resonant frequency ω_c. The lattice is formed by the coupling t_1 between the sublattices A and B and the coupling t_2 between the sublattices B and C. The Hamiltonian of the stub ribbon is

$$H_{\mathrm{stub}} = \sum_n [t_1 A_n^\dagger B_n + t_2 (B_n^\dagger C_n + C_n^\dagger B_{n+1})] + \mathrm{H.c.}, \qquad (10)$$

where $A_n^\dagger$, $B_n^\dagger$, and $C_n^\dagger$ (A_n, B_n, and C_n) denote the creation (annihilation) operators for the three sublattices in the nth unit cell. We plot the eigenenergies of a 30-site stub ribbon in Fig. 4(b). The stub ribbon has two dispersive bands and one zero-energy flat band in the middle. The flat band exhibits a tenfold degeneracy, which increases with the expansion of the lattice size. The wave function amplitudes for each site of the unnormalized eigenstate of the flat band are depicted in Fig. 4(a), which are compactly localized within two neighbor unit cells and have nonvanishing amplitudes only at the sublattices A and C. Notably, the flat band in the stub ribbon is protected by the chiral symmetry (see Supplemental Material, Sec. D [56]), rendering it independent of the coupling strengths. The chiral symmetry and flat band persist even in the presence of coupling disorder [76,77]. The eigenenergies in the presence of coupling disorder are shown in Fig. 4(c). The coupling disorder affects two dispersive bands, leading to the perturbations in their eigenenergies [78], while the zero-energy flat band is immune to the coupling disorder similarly as in the topological edge state [79]. The robustness is always desirable for practical applications [80–84].

Robust incoherent perfect absorber. To design a robust incoherent perfect absorber, the stub ribbon as the scattering center is connected to two semi-infinite coupled resonator chains (Fig. 5). The two resonator chains serve as the input and output ports, which are coupled to the sublattice C sites from *any* two different unit cells of the stub ribbon. The port coupling is $-J$ and the resonant frequency is ω_c.

We focus on the on-resonant incident wave with the momentum $k = \pi/2$. The steady-state solutions formed by the incident wave injected from the upper and lower ports into the stub ribbon are shown in Figs. 5(a) and 5(b), respectively. The losses at the connection resonators are $\gamma = J$. The propagation direction of the plane wave is indicated by the purple arrow. The uniform intensity observed at the input port reveals the presence of only incident waves, indicating the vanishing reflection. Moreover, the zero intensity at the output port indicates the vanishing transmission. The incident wave injected from the input port propagates without reflection to the output port until being absorbed at the connection resonators. The

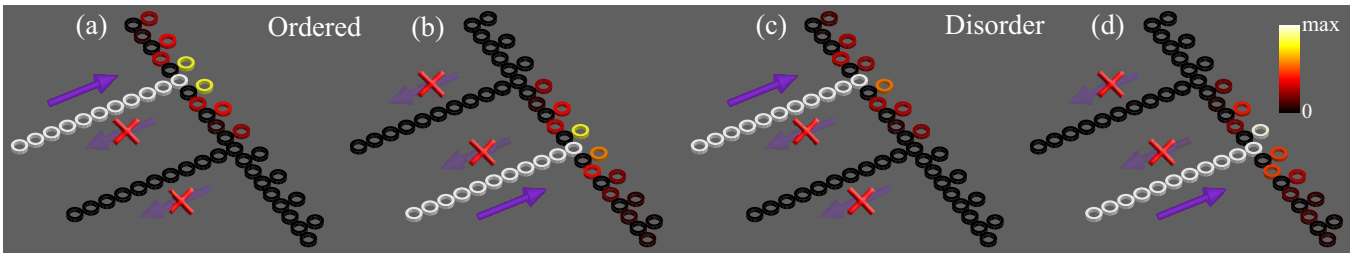

FIG. 5. The steady-state solutions for different incident directions [(a), (b)] without disorder and [(c), (d)] with disorder. The color bar indicates the intensity of wave function. The non-Hermitian stub ribbon is the stub ribbon in Fig. 4 with additional losses at the two connection sites. The port coupling is chosen $J = t_2$.

incident waves injected from different ports are both trapped within the stub ribbon and completely absorbed without any reflection or transmission. These demonstrate the incoherent perfect absorption.

The proposed incoherent perfect absorber, without the requirement of coherent input, exhibits robust high absorption efficiency. We emphasize that the zero-energy flat band is a key factor for the formation of incoherent perfect absorption in the stub ribbon. The superposition of compact localized states of the flat band as the incoming wave solution of the scattering system creates the destructive interference at the two connection resonators, respectively. This ensures the complete absorption of incoming waves injected from both directions. Furthermore, the flat band is maintained in the presence of random coupling disorder. Consequently, the incoherent perfect absorption is robust against the random coupling disorder although the distribution of the steady-state solutions within the stub ribbon is affected. The steady-state solutions in the presence of random coupling disorder are depicted in Figs. 5(c) and 5(d). In addition, the incoherent perfect absorption induced by the stub ribbon is also robust against the random detuning in the sublattice B (see Supplemental Material, Sec. E [56]).

The proposed approach for the construction of robust incoherent perfect absorbers can be applied to other quasi-one-dimensional systems such as the rhombic lattice [85–87] and the two-dimensional systems such as the Lieb lattice [88–90], including various of non-Hermitian flat-band lattices [91–98] . The incoherent perfect absorption is induced by the interplay between the engineered loss and flat-band localization. In addition, the incoherent perfect absorption protected by the specific symmetries demonstrates remarkable robustness to the disorder. The robust incoherent perfect absorption can be implemented in the coupled waveguides and other platforms [99].

Conclusion. We have found that the linearly independent destructive interference of the on-resonance degenerate eigenstates from the effective scattering center at the port connections creates the incoherent perfect absorption. The resonant inputs are completely absorbed without the requirement of a proper coherent input, which is beneficial for future applications. The degenerate eigenstates of the effective scattering center are required, but the inversion symmetry is not necessary [39]. Furthermore, we have proposed a robust incoherent perfect absorption using the flat-band localization. The proposed incoherent perfect absorption protected by the chiral symmetry is immune to the disorder, leading to the high absorption efficiency. Our findings are insightful for the perfect absorption of light, microwaves, sound, mechanical waves, and beyond.

Acknowledgment. This work was supported by National Natural Science Foundation of China (Grant No. 12222504).

[1] Y. D. Chong, L. Ge, H. Cao, and A. D. Stone, Coherent perfect absorbers: Time-reversed lasers, Phys. Rev. Lett. **105**, 053901 (2010).

[2] W. Wan, Y. Chong, L. Ge, H. Noh, A. D. Stone, and H. Cao, Time-reversed lasing and interferometric control of absorption, Science **331**, 889 (2011).

[3] S. Longhi and G. D. Valle, Coherent perfect absorbers for transient, periodic, or chaotic optical fields: Time-reversed lasers beyond threshold, Phys. Rev. A **85**, 053838 (2012).

[4] Y. Sun, W. Tan, H.-Q. Li, J. Li, and H. Chen, Experimental demonstration of a coherent perfect absorber with PT phase transition, Phys. Rev. Lett. **112**, 143903 (2014).

[5] D. G. Baranov, A. Krasnok, T. Shegai, A. Alù, and Y. Chong, Coherent perfect absorbers: Linear control of light with light, Nat. Rev. Mater. **2**, 17064 (2017).

[6] D. Zhang, X.-Q. Luo, Y.-P. Wang, T.-F. Li, and J. Q. You, Observation of the exceptional point in cavity magnon-polaritons, Nat. Commun. **8**, 1368 (2017).

[7] A. Müllers, B. Santra, C. Baals, J. Jiang, J. Benary, R. Labouvie, D. A. Zezyulin, V. V. Konotop, and H. Ott, Coherent perfect absorption of nonlinear matter waves, Sci. Adv. **4**, eaat6539 (2018).

[8] J. Jeffers, Nonlocal coherent perfect absorption, Phys. Rev. Lett. **123**, 143602 (2019).

[9] L. Chen, T. Kottos, and S. M. Anlage, Perfect absorption in complex scattering systems with or without hidden symmetries, Nat. Commun. **11**, 5826 (2020).

[10] Q. Zhong, L. Simonson, T. Kottos, and R. El-Ganainy, Coherent virtual absorption of light in microring resonators, Phys. Rev. Res. **2**, 013362 (2020).

[11] W. Xiong, J. Chen, B. Fang, C. Lam, and J. Q. You, Coherent perfect absorption in a weakly coupled atom-cavity system, Phys. Rev. A **101**, 063822 (2020).

[12] J. Luo, H. Chu, R. Peng, M. Wang, J. Li, and Y. Lai, Ultra-broadband reflectionless Brewster absorber protected by reciprocity, Light: Sci. Appl. **10**, 89 (2021).

[13] J. Hou, J. Lin, J. Zhu, G. Zhao, Y. Chen, F. Zhang, Y. Zheng, X. Chen, Y. Cheng, L. Ge, and W. Wan, Self-induced transparency in a perfectly absorbing chiral second-harmonic generator, PhotoniX **3**, 22 (2022).

[14] M. Liu, W. Chen, G. Hu, S. Fan, D. N. Christodoulides, C. Zhao, and C.-W. Qiu, Spectral phase singularity and topological behavior in perfect absorption, Phys. Rev. B **107**, L241403 (2023).

[15] F. Binkowski, F. Betz, R. Colom, P. Genevet, and S. Burger, Poles and zeros in non-Hermitian systems: Application to photonics, Phys. Rev. B **109**, 045414 (2024).

[16] A. Mostafazadeh, Spectral singularities of complex scattering potentials and infinite reflection and transmission coefficients at real energies, Phys. Rev. Lett. **102**, 220402 (2009).

[17] S. Longhi, $\mathcal{PT}$-symmetric laser absorber, Phys. Rev. A **82**, 031801(R) (2010).

[18] Y. D. Chong, L. Ge, and A. D. Stone, $\mathcal{PT}$-symmetry breaking and laser-absorber modes in optical scattering systems, Phys. Rev. Lett. **106**, 093902 (2011).

[19] Z. J. Wong, Y.-L. Xu, J. Kim, K. O'Brien, Y. Wang, L. Feng, and X. Zhang, Lasing and anti-lasing in a single cavity, Nat. Photonics **10**, 796 (2016).

[20] L. Ge and L. Feng, Contrasting eigenvalue and singular-value spectra for lasing and antilasing in a $\mathcal{PT}$-symmetric periodic structure, Phys. Rev. A **95**, 013813 (2017).

[21] V. V. Konotop and D. A. Zezyulin, Spectral singularities of odd-$\mathcal{PT}$-symmetric potentials, Phys. Rev. A **99**, 013823 (2019).

[22] V. V. Konotop, E. Lakshtanov, and B. Vainberg, Designing lasing and perfectly absorbing potentials, Phys. Rev. A **99**, 043838 (2019).

[23] S. Longhi, Photonic flat-band laser, Opt. Lett. **44**, 287 (2019).

[24] D. A. Zezyulin and V. V. Konotop, Universal form of arrays with spectral singularities, Opt. Lett. **45**, 3447 (2020).

[25] H. S. Xu and L. Jin, Coupling-induced nonunitary and unitary scattering in anti-$\mathcal{PT}$-symmetric non-Hermitian systems, Phys. Rev. A **104**, 012218 (2021).

[26] H. S. Xu, L. C. Xie, and L. Jin, High-order spectral singularity, Phys. Rev. A **107**, 062209 (2023).

[27] X. Fang, M. L. Tseng, J. Ou, K. F. MacDonald, D. P. Tsai, and N. I. Zheludev, Ultrafast all-optical switching via coherent modulation of metamaterial absorption, Appl. Phys. Lett. **104**, 141102 (2014).

[28] X. Fang, K. F. MacDonald, and N. I. Zheludev, Controlling light with light using coherent metadevices: All-optical transistor, summator and invertor, Light: Sci. Appl. **4**, e292 (2015).

[29] S. F. Liew, S. M. Popoff, S. W. Sheehan, A. Goetschy, C. A. Schmuttenmaer, A. D. Stone, and H. Cao, Coherent control of photocurrent in a strongly scattering photoelectrochemical system, ACS Photonics **3**, 449 (2016).

[30] F. Monticone, C. A. Valagiannopoulos, and A. Alù, Parity-time symmetric nonlocal metasurfaces: All-angle negative refraction and volumetric imaging, Phys. Rev. X **6**, 041018 (2016).

[31] T. Roger, S. Vezzoli, E. Bolduc, J. Valente, J. J. F. Heitz, J. Jeffers, C. Soci, J. Leach, C. Couteau, N. I. Zheludev, and D. Faccio, Coherent perfect absorption in deeply subwavelength films in the single-photon regime, Nat. Commun. **6**, 7031 (2015).

[32] T. Roger, S. Restuccia, A. Lyons, D. Giovannini, J. Romero, J. Jeffers, M. Padgett, and D. Faccio, Coherent absorption of N00N states, Phys. Rev. Lett. **117**, 023601 (2016).

[33] H. Ramezani, H.-K. Li, Y. Wang, and X. Zhang, Unidirectional spectral singularities, Phys. Rev. Lett. **113**, 263905 (2014).

[34] S. Longhi, Non-reciprocal transmission in photonic lattices based on unidirectional coherent perfect absorption, Opt. Lett. **40**, 1278 (2015).

[35] L. Jin and Z. Song, Incident direction independent wave propagation and unidirectional lasing, Phys. Rev. Lett. **121**, 073901 (2018).

[36] L. Jin, P. Wang, and Z. Song, Unidirectional perfect absorber, Sci. Rep. **6**, 32919 (2016).

[37] H. Ramezani, Y. Wang, E. Yablonovitch, and X. Zhang, Unidirectional perfect absorber, IEEE J. Sel. Top. Quantum Electron. **22**, 115 (2016).

[38] Y. Huang, Y. Shen, C. Min, S. Fan, and G. Veronis, Unidirectional reflectionless light propagation at exceptional points, Nanophotonics **6**, 977 (2017).

[39] J. R. Piper, V. Liu, and S. Fan, Total absorption by degenerate critical coupling, Appl. Phys. Lett. **104**, 251110 (2014).

[40] P. Bai, Y. Wu, and Y. Lai, Multi-channel coherent perfect absorbers, Europhys. Lett. **114**, 28003 (2016).

[41] J. Li, P. Yu, C. Tang, H. Cheng, J. Li, S. Chen, and J. Tian, Bidirectional perfect absorber using free substrate plasmonic metasurfaces, Adv. Opt. Mater. **5**, 1700152 (2017).

[42] Y. Slobodkin, G. Weinberg, H. Hörner, K. Pichler, S. Rotter, and O. Katz, Massively degenerate coherent perfect absorber for arbitrary wavefronts, Science **377**, 995 (2022).

[43] W. R. Sweeney, C. W. Hsu, S. Rotter, and A. D. Stone, Perfectly absorbing exceptional points and chiral absorbers, Phys. Rev. Lett. **122**, 093901 (2019).

[44] C. Wang, W. R. Sweeney, A. D. Stone, and L. Yang, Coherent perfect absorption at an exceptional point, Science **373**, 1261 (2021).

[45] A. Farhi, A. Mekawy, A. Alù, and D. Stone, Excitation of absorbing exceptional points in the time domain, Phys. Rev. A **106**, L031503 (2022).

[46] S. Soleymani, Q. Zhong, M. Mokim, S. Rotter, R. El-Ganainy, and S. K. Özdemir, Chiral and degenerate perfect absorption on exceptional surfaces, Nat. Commun. **13**, 599 (2022).

[47] C. Ferise, P. del Hougne, S. Félix, V. Pagneux, and M. Davy, Exceptional Points of $\mathcal{PT}$-symmetric reflectionless states in complex scattering systems, Phys. Rev. Lett. **128**, 203904 (2022).

[48] S. Suwunnarat, Y. Tang, M. Reisner, F. Mortessagne, U. Kuhl, and T. Kottos, Non-linear coherent perfect absorption in the proximity of exceptional points, Commun. Phys. **5**, 5 (2022).

[49] J. Sol, D. R. Smith, and P. del Hougne, Meta-programmable analog differentiator, Nat. Commun. **13**, 1713 (2022).

[50] Z. Sakotic, P. Stankovic, V. Bengin, A. Krasnok, A. Alù, and N. Jankovic, Non-Hermitian control of topological scattering singularities emerging from bound states in the continuum, Laser Photonics Rev. **17**, 2200308 (2023).

[51] J. Han, C. Gneiting, and D. Leykam, Helical transport in coupled resonator waveguides, Phys. Rev. B **99**, 224201 (2019).

[52] W. R. Sweeney, C. W. Hsu, and A. D. Stone, Theory of reflectionless scattering modes, Phys. Rev. A **102**, 063511 (2020).

[53] H. S. Xu and L. Jin, Coherent resonant transmission, Phys. Rev. Res. **4**, L032015 (2022).

[54] L. Jin and Z. Song, Symmetry-protected scattering in non-Hermitian linear systems, Chin. Phys. Lett. **38**, 024202 (2021).

[55] C. Guo and S. Fan, Reciprocity constraints on reflection, Phys. Rev. Lett. **128**, 256101 (2022).

[56] See Supplemental Material at http://link.aps.org/supplemental/10.1103/PhysRevResearch.6.L022006 for detailed calculations of scattering coefficients, the analytical expression of the minimum absorptance, an example of a coherent perfect absorber, the flat band and compact localized states of the stub ribbon, and steady-state solutions in the presence of detuning.

[57] H. S. Xu and L. Jin, Pseudo-Hermiticity protects the energy-difference conservation in the scattering, Phys. Rev. Res. **5**, L042005 (2023).

[58] The plane wave injection has a Gaussian profile $|\phi(0)\rangle = \Omega^{-1/2}\sum_j e^{-(j-N_c)^2/(2\sigma^2)}e^{ik_c j}|j\rangle$, where Ω is the normalization factor, σ controls the width, N_c is the spatial center, and k_c is the central momentum. The Gaussian wave packet input from either side toward the scattering center is completely absorbed without any reflection and transmission.

[59] L. Jin and Z. Song, Physics counterpart of the $\mathcal{PT}$ non-Hermitian tight-binding chain, Phys. Rev. A **81**, 032109 (2010).

[60] L. Jin and Z. Song, Partitioning technique for discrete quantum systems, Phys. Rev. A **83**, 062118 (2011).

[61] D. Leykam, A. Andreanov, and S. Flach, Artificial flat band systems: From lattice models to experiments, Adv. Phys.: X **3**, 1473052 (2018).

[62] D. Leykam and S. Flach, Perspective: Photonic flatbands, APL Photonics **3**, 070901 (2018).

[63] L. Tang, D. Song, S. Xia, S. Xia, J. Ma, W. Yan, Y. Hu, J. Xu, D. Leykam, and Z. Chen, Photonic flat-band lattices and unconventional light localization, Nanophotonics **9**, 1161 (2020).

[64] J. Ma, J. Rhim, L. Tang, S. Xia, H. Wang, X. Zheng, S. Xia, D. Song, Y. Hu, Y. Li, B. Yang, D. Leykam, and Z. Chen, Direct observation of flatband loop states arising from nontrivial real-space topology, Phys. Rev. Lett. **124**, 183901 (2020).

[65] Y. Xie, L. Song, W. Yan, S. Xia, L. Tang, D. Song, J. Rhim, and Z. Chen, Fractal-like photonic lattices and localized states arising from singular and nonsingular flatbands, APL Photonics **6**, 116104 (2021).

[66] R. A. V. Poblete, Photonic flat band dynamics, Adv. Phys.: X **6**, 1878057 (2021).

[67] S. Flach, D. Leykam, J. D. Bodyfelt, P. Matthies, and A. S. Desyatnikov, Detangling flat bands into Fano lattices, Europhys. Lett. **105**, 30001 (2014).

[68] C. Gneiting, Z. Li, and F. Nori, Lifetime of flatband states, Phys. Rev. B **98**, 134203 (2018).

[69] S. M. Zhang and L. Jin, Compact localized states and localization dynamics in the dice lattice, Phys. Rev. B **102**, 054301 (2020).

[70] S. M. Zhang, H. S. Xu, and L. Jin, Tunable Aharonov-Bohm cages through anti-$\mathcal{PT}$-symmetric imaginary couplings, Phys. Rev. A **108**, 023518 (2023).

[71] D. Leykam, S. Flach, and Y. D. Chong, Flat bands in lattices with non-Hermitian coupling, Phys. Rev. B **96**, 064305 (2017).

[72] L. Ge, Parity-time symmetry in a flat-band system, Phys. Rev. A **92**, 052103 (2015).

[73] F. Baboux, L. Ge, T. Jacqmin, M. Biondi, E. Galopin, A. Lemaître, L. L. Gratiet, I. Sagnes, S. Schmidt, H. E. Türeci, A. Amo, and J. Bloch, Bosonic condensation and disorder-induced localization in a flat band, Phys. Rev. Lett. **116**, 066402 (2016).

[74] L. Ge, Non-Hermitian lattices with a flat band and polynomial power increase, Photonics Res. **6**, A10 (2018).

[75] G. Li, L. Wang, R. Ye, S. Liu, Y. Zheng, L. Yuan, and X. Chen, Observation of flat-band and band transition in the synthetic space, Adv. Photonics **4**, 036002 (2022).

[76] H. Vemuri, V. Vavilala, T. Bhamidipati, and Y. N. Joglekar, Dynamics, disorder effects, and $\mathcal{PT}$-symmetry breaking in waveguide lattices with localized eigenstates, Phys. Rev. A **84**, 043826 (2011).

[77] M. Horodynski, M. Kühmayer, C. Ferise, S. Rotter, and M. Davy, Anti-reflection structure for perfect transmission through complex media, Nature (London) **607**, 281 (2022).

[78] D. Leykam, S. Flach, O. Bahat-Treidel, and A. S. Desyatnikov, Flat band states: Disorder and nonlinearity, Phys. Rev. B **88**, 224203 (2013).

[79] H. C. Wu, H. S. Xu, L. C. Xie, and L. Jin, Edge state, band topology, and time boundary effect in the fine-grained categorization of Chern insulators, Phys. Rev. Lett. **132**, 083801 (2024).

[80] Y. N. Joglekar, D. Scott, M. Babbey, and A. Saxena, Robust and fragile $\mathcal{PT}$-symmetric phases in a tight-binding chain, Phys. Rev. A **82**, 030103(R) (2010).

[81] Y. N. Joglekar and A. Saxena, Robust $\mathcal{PT}$-symmetric chain and properties of its Hermitian counterpart, Phys. Rev. A **83**, 050101(R) (2011).

[82] F. Zangeneh-Nejad and R. Fleury, Topological Fano resonances, Phys. Rev. Lett. **122**, 014301 (2019).

[83] M. Reisner, D. H. Jeon, C. Schindler, H. Schomerus, F. Mortessagne, U. Kuhl, and T. Kottos, Self-shielded topological receiver protectors, Phys. Rev. Appl. **13**, 034067 (2020).

[84] M. Koppenhöfer, P. Groszkowski, and A. A. Clerk, Squeezed superradiance enables robust entanglement-enhanced metrology even with highly imperfect readout, Phys. Rev. Lett. **131**, 060802 (2023).

[85] M. Kremer, I. Petrides, E. Meyer, M. Heinrich, O. Zilberberg, and A. Szameit, A square-root topological insulator with non-quantized indices realized with photonic Aharonov-Bohm cages, Nat. Commun. **11**, 907 (2020).

[86] C. Jörg, G. Queraltó, M. Kremer, G. Pelegrí, J. Schulz, A. Szameit, G. V. Freymann, J. Mompart, and V. Ahufinger, Artificial gauge field switching using orbital angular momentum modes in optical waveguides, Light: Sci. Appl. **9**, 150 (2020).

[87] G. Cáceres-Aravena, D. Guzmán-Silva, I. Salinas, and R. A. Vicencio, Controlled transport based on multiorbital Aharonov-Bohm photonic caging, Phys. Rev. Lett. **128**, 256602 (2022).

[88] D. Leykam, O. Bahat-Treidel, and A. S. Desyatnikov, Pseudospin and nonlinear conical diffraction in Lieb lattices, Phys. Rev. A **86**, 031805(R) (2012).

[89] S. Mukherjee, A. Spracklen, D. Choudhury, N. Goldman, P. Öhberg, E. Andersson, and R. R. Thomson, Observation of a localized flat-band state in a photonic Lieb lattice, Phys. Rev. Lett. **114**, 245504 (2015).

[90] R. A. Vicencio, C. Cantillano, L. Morales-Inostroza, B. Real, C. Mejía-Cortés, S. Weimann, A. Szameit, and M. I. Molina, Observation of localized states in Lieb photonic lattices, Phys. Rev. Lett. **114**, 245503 (2015).

[91] M. I. Molina, Flat bands and $\mathcal{PT}$ symmetry in quasi-one-dimensional lattices, Phys. Rev. A **92**, 063813 (2015).

[92] H. Ramezani, Non-Hermiticity-induced flat band, Phys. Rev. A **96**, 011802(R) (2017).

[93] B. Qi, L. Zhang, and L. Ge, Defect states emerging from a non-Hermitian flatband of photonic zero modes, Phys. Rev. Lett. **120**, 093901 (2018).

[94] T. Biesenthal, M. Kremer, M. Heinrich, and A. Szameit, Experimental realization of $\mathcal{PT}$-symmetric flat bands, Phys. Rev. Lett. **123**, 183601 (2019).

[95] L. Jin, Flat band induced by the interplay of synthetic magnetic flux and non-Hermiticity, Phys. Rev. A **99**, 033810 (2019).

[96] S. M. Zhang and L. Jin, Flat band in two-dimensional non-Hermitian optical lattices, Phys. Rev. A **100**, 043808 (2019).

[97] S. M. Zhang and L. Jin, Localization in non-Hermitian asymmetric rhombic lattice, Phys. Rev. Res. **2**, 033127 (2020).

[98] W. Maimaiti and A. Andreanov, Non-Hermitian flat-band generator in one dimension, Phys. Rev. B **104**, 035115 (2021).

[99] B.-C. Xu, B.-Y. Xie, L.-H. Xu, M. Deng, W. Chen, H. Wei, F. Dong, J. Wang, C.-W. Qiu, S. Zhang, and L. Chen, Topological Landau-Zener nanophotonic circuits, Adv. Photonics **5**, 036005 (2023).